Thermal building control using active ventilated block integrating phase change material

Amine Laaouatni, Nadia Martaj, Rachid Bennacer, Mohammed Lachi, Mohamed El Omari, Mohammed El Ganaoui

Thermal building control using active ventilated block integrating phase change material

Amine Laaouatni[1, 2], Nadia Martaj[1, 3], Rachid Bennacer[4, 5, *], Mohammed Lachi[3], Mohamed El Omari[2] and Mohammed El Ganaoui[6]

[1]EPF Campus de Troyes 2, rue F. Sastre 10430 Rosières-près-Troyes, France

[2]Laboratory of Automation, Environment and Transfer Processes LAEPT, Faculty of Sciences Semlalia, Cadi Ayyad University, P. B. 2390, Marrakesh, Morocco

[3]GRESPI EA 4694, University of Reims Champagne Ardenne, UFR Sciences Exactes et Naturelles, Moulin de la Housse, 51687 Reims cedex 2, France

[4]LMT-Cachan, ENS Cachan CNRS, Université Paris Saclay, 61 avenue du Président Wilson, 94230 Cachan, France

[5]ECAM EPMI, Cergy Pontoise, France

[6]Université de Lorraine, Laboratoire Lermab-longwy, IUT Henri Poincaré de Longwy, 186 rue de Lorraine, 54400 Longwy - Cosnes et Romain, France

***Corresponding author**

Email: rachid.bennacer@ens-cachan.fr

Keywords: Phase change material (PCM), Thermal building, Modelling, Thermal modelling, Thermal inertia.

Abstract

In the context of improving energy efficiency and thermal comfort in the building, the use of phase change materials (PCMs) is one of the suggested solutions. The proposed integration solutions concern the building envelope as well as the applications related to its operation. The study of the incorporation of PCM in the walls of the building was the subject of numerous works. However, the antisymmetric character of storing/recovering energy management in the walls is less controlled and do not fit the optimal conditions. In this study, a solution based on the direct integration of a stabilized PCM (gel) in an envelope including ventilation channels, was proposed to overcome this problem of antisymmetry storing/recovering and fitting with different fixed ambient conditions. The final aim is to develop the optimization strategy of a wall combining the heavy inertia offered by the PCM, intra-ventilation control and the contribution to air renewal energy demand.

In this context, an experimental study of a concrete block system is conducted to test the thermal response of this configuration by the application of cyclic solicitations. The comprehension of this integrated constructive solution essentially passes by the possession of validated numerical tools. For this, two models have been developed. The first model using the electrical-thermal analogy, based on an RC equivalence, is distinguished by its relative simplicity and weak time computing demand. Each of these two factors, R and C summarise the system properties and has a direct influence on the building transient simulations over a year. The second one is based on direct numerical simulation DNS of the energy and fluid flow equations using commercial code COMSOL Multiphysics. Such DNS is time consuming and could not be used to simulate over a year but aims only to validate the first RC circuit approach. A comparison of these two models with the idealised experimental data was carried out and allowed the validation of the thermal behaviour of the solution based on the integration of the PCM with core ventilation.

Nomenclature

Latin letters

f_v *Volume fraction*

C *Thermal capacitance (J/K)*

C_p *Specific heat at constant pressure (J/kg* K)

e *Element thickness (m)*

h *Convective heat transfer coefficient (W/m² K)*

k *Thermal conductivity (W/m K)*

L *Length (m)*

$\dot{m}$ *Airflow rate (kg/s)*

Q *Heat flux (W/m²)*

R *Thermal resistance (K/W)*

Ra *Rayleigh number*

S *Surface (m²)*

T *Temperature (K, °C)*

t *Time (s)*

T_{in} *Air inlet temperature (K, °C)*

T_{om} *Onset temperature of the melting (K, °C)*

T_{ou} *Air outlet temperature (K, °C)*

T_{sl} *Phase change temperature (K, °C)*

u *Velocity field (m/s)*

Greek letters

ΔL *Latent heat (J/kg)*

ε *Emissivity*

μ *Dynamic viscosity (kg/m s)*

ρ *Density (kg/m³)*

σ *Stefan-Boltzmann constant (W/m² K⁴)*

φ *Solar radiation heat flux (W/m²)*

Subscripts

amb *Ambient*

$_{conv}$ *Convection*

c *Concrete*

$elec$ *Referring to electrical physical quantities*

i *Internal, indoor*

l *Liquid*

min Minimum

o *Outer, outdoor*

pcm *Phase change material*

rad *Radiation*

s *Solid*

t *Tube*

v *Ventilation*

w *Wall*

Acronyms

EXP *Referring to experimentation*

FEM *Finite element model*

DSC *Differential scanning calorimetry*

PCM *Phase change material*

PVC *Polyvinyl chloride*

RC *Referring to resistance and capacitance network model*

1. Introduction

Energy consumption in the building sector is gaining increasing interest as it is directly related to energy economics and sustainable development. The design and the choice of building materials, as well as the energy and thermal systems evolve very rapidly. In the energy challenge, the building is among the largest consumers of energy. Efficiency and optimization of energy systems remain among the main axes studied in order to reduce energy consumption and increase system performance. The need to balance available energy with occupant comfort involves the use of new innovative and effective technological solutions. In the area of housing, the cost and optimization of space are the two main reasons that require the decrease of the thickness of walls in new constructions; however,

this reduction greatly affects the thermal inertia of the frame and makes it insufficient to effectively damp the oscillations due to the outdoor temperature variation. Moreover, the management of thermal comfort by control systems acting on ventilation poses the problem of increasing the electrical consumption energy and the drawbacks related to the operation of these devices (noise, maintenance, etc.).

The integration of phase change materials (PCMs) in the building envelope is an interesting solution to optimize energy consumption. When integrated into building elements, their energy storage capacity using latent heat is manifested. A thermal phase shift is performed during the energy storage phase, then comes the restitution phase with a damping, which reduces the needs according to the outdoor climatic conditions of the considered construction. This topic has been the subject of numerous studies aimed at answering the various difficulties that oppose the optimal use of this solution [1–4]. Among these constraints, one can cite the choice of the appropriate method of incorporation of these products but also the limits imposed by the use of such a material which changes phase. Direct incorporation, impregnation of building materials, incorporation of capsules filled with PCM are part of the used methodologies. Thus, in order to minimize the risk of leakage during the melting of this type of product, mixtures are used which aim at reinforcing the PCM matrix, for example, the use of polymers which make it possible to have mechanically stable gels during the process liquid phase [5]. Similarly, the efficiency of the systems developed requires an optimization study on the types of PCM to be used, the dimensions of the system and the possible combinations in order to correctly manage the energy charged/discharged in these products [6,7].

Two categories of integration can be distinguished, when incorporated into the building envelope or in applications related to the thermal comfort regulation during the occupation of the building. In the first type of integration, the following cases can be mentioned: integration in floors [8–10], walls [11–13], masonry elements [14–16] and roofs [17–19]. This integration category of PCM also includes its use in windows and glazing [20–22] as well as in shading systems [23–25]. Concerning the use of PCMs in comfort conditioning systems within the building, the free cooling method based on heat exchangers was developed according to several approaches [26–29]. These different studies have shown that the contribution of PCMs increases the thermal inertia and on the other hand improves the air quality in buildings.

The vertical elements of the building are the most studied, the wall panels that can be fixed on the base walls are among the solutions proposed. In this context, many products have been tested and marketed because this solution makes it possible to minimize the level of the peak temperature during hot periods and to save energy. The damping of the peaks of temperature obtained can go up to 4°C [30–32]. Concrete and coatings PCM based are part of the solutions applied to the walls. They are found under several compositions with different percentages of PCM. The tests carried out in a real scale on cells, show the increase

of the storage capacity as a function of the volume ratio of the PCMs, as well as the difference in indoor surface temperature with respect to a reference cell [12,33,34].

The solutions applied to the walls also include integration into the masonry elements. In this configuration Alawdhi *et al.* [7] conducted an optimization study of the amount of PCM to be introduced into bricks containing cylindrical cavities. By means of a 2D finite element model, they show that the best configuration reduces the inward heat flux on the wall by 17.55%. Zhang *et al.* [14] numerically studied the filling of holes in traditional bricks. As results, the study shows a 10% decrease in the amplitude of the surface temperature of the wall. Principi *et al.* [15] presented an experimental and theoretical study of the impact of a brick wall with PCM. As result, they showed that the presence of PCM affects the peak of heat and it generates a phase shift of 6 hours with a decrease of 25% of temperature amplitude.

In all these works on construction materials, the interest is on the behaviour of the PCM mainly in relation to the quantity used and the different combinations of filling in order to obtain the best possible configuration [35]. However, these applications do not allow the control and management of the stored/recovered energy in the PCM other than the change in quantities or the type of PCM. The PCM imposes its behaviour on the output indicators, which reflect the response of the system. A wall containing PCM is solicited from the outside by an oscillating temperature between two, maximum and minimum values influenced by the solar heat flux, while the interior is restricted by a comfort temperature generally set by conditioning systems that operate for compensating or eliminate the heat flux crossing the walls. In summer, the heat loads crossing the wall can be considered negligible if compared to the internal heat gains. Such heat loads are shifted during the night hours. The increase in apparent heat capacity and a fast discharge will act and enhance the indoor comfort as it is equivalent to efficient free cooling.

Often, the chosen phase change temperature is generally close to the comfort set point, this remains valid as long as the PCM part is close to the inner side. Depending on the season and weather conditions, charging and discharging a PCM-based wall does not occur at the same time. In this situation, a rebalancing is necessary in order to accelerate or slow down the charging period or to shift the discharge.

As part of this study, a new strategy is proposed for using a wall with PCM, adding internal ventilation through tubes located within the PCM contained in the wall. Fig. 1 shows the wall which consists of concrete blocks filled with PCM and ventilated channels. This solution allows both increasing the thermal inertia thanks to the inertial capacity of the PCM and to control the charge/discharge while enhancing the exchanges by injecting the air from the outside to the inside. It thus allows contributing to the conditioning of the renewal of the local air and the temperature change. The diagram presented in Fig. 1 also shows the utility of such a system in the management of energy needs. It allows, for example, the storage of the energy released during the night from heating [36]. Ventilation control through the system helps to meet some of the morning's energy needs when occupants wake up.

Fig. 1. Principle and utility of the tubes in the developed solution.

The study of thermal solutions in the building usually goes through an experimental study which serves as a basis for validation of the models and optimization on the numerical level. The development of the numerical model is essential to show the usefulness of the solutions and quantify the thermal behaviour of the systems. However, the resolution of the studied physical system requires techniques based on equations describing the physical behaviour of heat transfer. Generally, three main thermal building models are currently used in modelling: multi-zone, zonal and CFD (Computational Fluid Dynamics) methods [37].

In the multi-zone or nodal approach, modelling by electrical analogy is a technique often used. It simplifies the physical problem by linearizing the equations and thus reduces the calculation time. The equivalent electric circuit, formed of resistances and capacitances (RC), represents the fundamental physical relations which translate the studied thermal phenomena. It is based on the combination of a thermal resistance *R* and a thermal capacity *C* for each studied thermal element. The RC model is distinguished by its speed, which is an important factor in simulations related to the building where the heat exchanges require substantial time intervals where calculations generally become very heavy [38–43]. In addition to the phenomena often modelled, namely conduction and convection, a modelling of the phase change of paraffin with integrated ventilation system will be presented in this study. The features of the Simscape library integrated in the Matlab/Simulink environment are used. The method of resolution, thus adopted makes it possible to work on a circuit constituted of variable resistances and capacitances.

This article is part of the studies on the direct integration of a phase change material into a concrete block [44,45]. In this context, a structural element of "hollow concrete block" filled with a polymer-paraffin composite and provided with ventilation tubes allowing the circulation of air will be studied. The used mixture of PCM is mechanically stable and that avoids the problem of leakage. This study will be presented in four main axes:

- The first one is developed in approaching the actual operating conditions of the system and represents the experimental study which is used to compare the effect of PCM filling and the influence of tube condition (open, closed and ventilated).
- The second part is dedicated to modelling of the system under COMSOL Multiphysics.
- After validating the used model, the third part will be devoted to reducing the time calculation request by using the electrical analogy modelling and the equivalent RC model.
- Finally, a validation was performed by comparing the two models with the experimental data.

2. System description

Fig. 2(a) presents a diagram and an illustration of the developed system which is based on a commercial hollow Concrete Block having the following length x height x width dimensions: 50 cm x 20 cm x 9.5 cm. The concrete block consists of 3 parallelepiped cavities. A PVC tubes are used, with a diameter of 2 cm and a thickness of 1 mm. Two holes are carried out in the base of each cavity to place the six tubes. The PCM is incorporated directly in the molten state in the cavities (temperature higher than the temperature of the solid gel).

Fig. 2. Description of the developed system: **(a)** Schematic of the ventilated hollow concrete block integrating PCM **(b)** Schematic diagram of the experimental setup.

The used PCM is a mixture of paraffin and a styrene-type polymer. The choice of paraffin removed both hydrated salts, known by their corrosive tendency, as well as unsuitable fatty acids because in our case the PCM is directly put in contact with the concrete having a basic pH. The use of a percentage of polymers in solution makes it possible to obtain a gel with acceptable stability in order to avoid problems of leakage in the liquid state. Currently, paraffin manufacturers offer a wide range that varies with melting temperature as well as latent heat. Normally, the choice will have to take into consideration the antisymmetry between the external conditions and the temperature of comfort fixed indoor. The melting temperature chosen is important to create a wall temperature stabilization bearing close to that of comfort and also offer a sufficient storage that allows the incoming air to be conditioned through the tubes. The realized mixture has the same characteristics as that used in the work of Royon et al. [5]. Base paraffin is a commercial product having a melting temperature of 27 °C and a latent heat of 179 *kJ/kg*. This choice is also based on experimental laboratory manipulation conditions, which requires a difference between the melting temperature and the ambient temperature to avoid the onset of melting. The percentage of the used polymer is of 15%. The latent heat after mixing is equal to 110 *kJ/kg*. Table 1 summarizes the characteristics of the mixture as well as the materials constituting the used system.

Table 1. Thermo-physical properties of the materials constituting the system.

3. Experimental study

This part is devoted to the description of the used experimental device as well as the procedure explaining the progress of the realized tests.

The obtained results of the experimental study are presented and a comparative study of the different mounting configurations chosen is carried out to show the system behaviour.

3.1. Experimental device and procedure

Using a real scale system imposes constraints to fully adapt the experimental study and the actual operation of the considered element as a representative part of a sunny wall. The

experimental device consists of an electrical resistance which allows imposing a power heat on the side surface of the concrete block. K-type thermocouples are arranged on both side surfaces, they are placed at mid-height and on the same horizontal plane (Fig. 2(b)). Linked to the acquisition system, they make it possible to follow the evolution of the temperature. Small fans are used to inject air through the tubes. The speed and temperature of the air are checked with a hot-wire anemometer. In order to avoid thermal losses at the edges of the system, a layer of polyurethane foam surrounds the other surfaces is used. The second face of the block is in contact with the ambient air of the laboratory room which varies slightly around 21 °C.

A preliminary study of thermal stresses allowed choosing an adequate heating power so as not to exceed a temperature of 50 °C on the heated surface. This maximum temperature is chosen relative to the limit of the stability of the used gel. The solicitation chosen has three cycles with a duration of 24 hours for each one. Each cycle consists of applying a constant heat power for 5 to 6 hours, except for the concrete block without PCM which its inertia is too low and this duration of cycle is reduced in this case. After stopping the thermal solicitations, a normal cooling is applied for the rest of the cycle for all configurations, except in the case with forced ventilation; the air injection is activated directly after halting. The experimental device as presented in Fig. 3, allows simulation the operating principle of each studied element. Also, this installation would serve as a basis for the development and validation of a complete numerical tool.

Fig. 3. Photography of the experimental bench.

3.2. *Experimental results*

The adopted experimental methodology makes it possible to follow the evolution of the temperatures by the application of three identical cycles of heat fluxes. The use of cyclic stresses allows testing the thermal behaviour of the PCM over a more prolonged period. The finding of each configuration is presented in Fig. 4. The curves show the temperature evolutions recorded on the lateral surface in contact with the ambient air. The heat flux is imposed in the same way for all configurations. However, the experimental protocol makes that the operating intervals are different according to the configuration tested. The threshold temperature of 50 °C is the basis for the control of the electrical resistance which simulates the sunshine and not the duration of application of the thermal stresses, which is the result of the inertia and the thermal behaviour of each configuration. Two systems are studied here; empty concrete block without PCM and system with PCM and tubes. For the second system, three cases can be distinguished according to the state of the tubes which can be, closed, opened or ventilated.

Fig. 4. Evolution of the temperature on the lateral surface of the concrete block for different configurations.

The analysis of temperature evolution from the third cycle as represented in Fig. 5, shows the effect of PCM filling. On the one hand, it contributes to the increase in the phase shift from 0.5 hour in the case without PCM to 3.8 hours; on the other hand, the PCM allows the reduction of recorded temperature peaks of about 3.4 °C. The study of the state of the tubes on the response of the wall shows that the decrease in the recorded maximum temperature is a function of the transfer mode imposed through the tubes.

In the case where tubes are closed, the response of the system is explained by the predominance of conduction due to the diameter of the tubes that does not promote the establishment of the convection heat transfer. When the tubes are open, in this case, they favour a convective heat exchange thanks to the difference in density of the air between the inside and the outside of the tubes; this small contribution explains the decrease in the temperature evolution. Forced convection induces by the air injection further enhances system response. The ventilation allows lowering the temperature level quickly on the inner surface; a decrease of temperature from 3.4 to 4.7 °C compared to the case without PCM. This gain in temperature is accompanied by a decrease in phase shift time from 3.8 to 2.9 hours which is a normal result because the application of ventilation improves the discharging by a withdrawal of energy and thus induces a cooling of the system too. This behaviour also explains the ability of the ventilated system to store more energy, which therefore increases the necessary time to reach the threshold temperature on the heated surface. The curves show (Fig. 5) that it takes 6.5 instead of 4.5 hours for the system without ventilation, while only 2.4 hours are needed for the concrete block without PCM.

Fig. 5. Temperature analysis on the lateral surface of the concrete block for the different configurations starting from the third cycle.

The temperature of the outgoing air measured by the hot-wire anemometer shows that the maximum increase thereof reaches about 10 °C during the exchange of the discharged energy through the tubes. This operating scenario makes it possible to heat the incoming air from the outdoor by supplying the energy recovered on the PCMs during the renewal of air. The response of the complete system with ventilated tubes shows that the discharging of the energy is not sufficient to reach the same temperature at the end of the cycle in the case without PCM. These results clearly demonstrate the role of PCMs in energy storage and the efficiency of the recovery system by the ventilated tubes. However, an optimization study on the quantity of PCM and the characteristics of the tubes will allow finding the best configuration with the experimental used conditions.

4. Numerical simulation

As part of phase change problems solving, the use of COMSOL Multiphysics has demonstrated good correlations with experimental results [46–48]. It allows the solving of problems governed by partial differential equations by the finite element method. The formulation using apparent specific heat approach is used to model the phase change [49].

Three-dimensional modelling (3D) has been developed in this study. The partial differential equation that governs heat transfer in the model is given by Eq. (1).

$$(\rho C_P)(\frac{\partial T}{\partial t} + u\nabla T) = \nabla(k\nabla T) \quad (1)$$

where ρ, C_p and k are the intrinsic characteristics of the concerned material, u is the velocity field. The main characteristics of the PCM are evaluated experimentally. The different thermo-physical properties of the materials (Table 1) are introduced into the modelling. The thermo-physical properties of the PCM are governed by Eqs. (2)–(6).

$$k_{pcm} = f_v k_s + (1-f_v)k_l \quad (2)$$

$$\rho_{pcm} = f_v \rho_s + (1-f_v)\rho_l \quad (3)$$

$$C_{p\,pcm} = \frac{f_v(\rho C_p)_s + (1-f_v)(\rho C_p)_l}{\rho_{pcm}} + \frac{\partial \alpha_m}{\partial T} \times \Delta L \quad (4)$$

$$\theta = \begin{cases} 1 & ; \ T < T_{sl} - \Delta T/2 \\ \dfrac{T - Tsl}{\Delta T} + 0.5 & ; \ T_{sl} - \dfrac{\Delta T}{2} \le T \le T_{sl} + \dfrac{\Delta T}{2} \\ 0 & ; \ T > T_{sl} + \Delta T/2 \end{cases} \quad (5)$$

$$\alpha_m = \begin{cases} -1/2 & ; \ T < T_{sl} - \Delta T/2 \\ \dfrac{(1-f_v)\rho_l - f_v \rho_s}{2 \times \rho_{pcm}} & ; \ T_{sl} - \dfrac{\Delta T}{2} \le T \le T_{sl} + \dfrac{\Delta T}{2} \\ 1/2 & ; \ T_{sl} + \Delta T/2 \end{cases} \quad (6)$$

where f_v is the volume fraction of the PCM solid phase, ΔT is the phase transition interval, T_{sl} is the phase change temperature and α_m is the mass fraction defined from ρ_s, ρ_l and f_v.

The considered boundary conditions are as follows: on the heated side surface, a homogeneous temperature corresponding to the average temperature recorded experimentally was imposed. On the other side surface, a convective exchange with the ambient environment was used. The convective transfer coefficient, h_{con} between the lateral surface of the block and the ambient air, is calculated by Eq. (7).

$$h_{conv} = \frac{Nu\, k_{air}}{L_w} \quad (7)$$

where Nu is the Nusselt number, k_{air} is the air thermal conductivity and L_w is the characteristic length of the surface of the concrete block. In our case, the flow is laminar and Nu is calculated from the correlation on a vertical plane [50] as:

$$Nu = 0.59 \times Ra^{1/4} \tag{8}$$

The convection coefficient h_{con} calculated with the correlation is equal to 3.3 *W/m².K*. In addition to the convective effects, the lateral surface is subject to the phenomenon of radiation where the radiation heat flux is written as:

$$Q_{rad} = \varepsilon\sigma\left(T_w^4 - T_{amb}^4\right) \tag{9}$$

where ε is the emissivity of the concrete block which takes as value 0.9.

For modelling the case without ventilation, it is considered that the diameters of the tubes do not allow the appearance of a significant convective mode. However, the injection of ambient air, with the fans through the tubes, is activated with a measured speed of 1.3 *m/s*. The calculation of the Reynolds number Re shows that the regime is laminar. The studied model has short diameter pipes; which imposes to take into account the effects of the inlet region, the correlation of Seider and Tate [51] is used to calculate the Nusselt number Nu inside the tube:

$$N_{ut} = 1.86 \times \left(Re \times Pr \frac{D_i}{L_t} \right)^{0.33} \left(\frac{\mu}{\mu_{wt}} \right)^{0.14} \tag{10}$$

Dynamic viscosity μ and the Prandtl number P_r are evaluated at the average temperature of the air between the inlet and the outlet of the tube. Thus, μ_{wt} is the viscosity of the air determined for the wall temperature of the tube T_{wt}. D_i and L_t represent respectively the inside diameter and the length of the pipe. As of the correlation, the forced convection coefficient through the tube is set equal to 11.7 (*W/m².K*). On the other surfaces of the concrete block; a zero heat flow condition is used (adiabatic surface).

5. Modelling by electrical analogy

It becomes a classical approach in order to simplify a thermal system and predict the temperature evolution over time under the control-command strategy. First, the principle of thermo-electric analogy and the decomposition of the system into a unitary element will be presented. After that, the modelling of the system will be detailed.

5.1. *Principle of thermal modelling by electrical analogy*

Thermal modelling by electrical analogy is based on the analogy with Ohm's law in electricity. The temperature and the heat flux play respectively in this problem the same role as the potential and the current in electricity. It is, therefore, possible to adopt for the thermal resistances the same representation as for the electrical resistances. As the electrical and thermal systems are similar, going from one system to another is possible while respecting the equivalences existing between the different components (Fig. 6).

Fig. 6. Equivalent electrical circuit (1R1C) in the unsteady case.

Assuming the unidirectional transfer of heat, the conductive heat flux Q, through a layer of a thick wall e_w, under the influence of a temperature difference $\Delta T = T_{wo} - T_{wi}$ is written as:

$$Q = \frac{k\,S}{e_w}\left(T_{wo} - T_{wi}\right) \tag{11}$$

In electricity, the application of a potential difference ΔV to a similar element is governed by Ohm's law, the electric current I is equivalent to the heat flux and it is expressed as:

$$I = \frac{\sigma S}{e_w}\Delta V = \frac{1}{R_{elec}}\Delta V \tag{12}$$

According to the two equations (11) and (12), the similarity with the electrical resistance allows to define the thermal resistance of conduction R (*K/W*):

$$R = \frac{e_w}{k\,S} \tag{13}$$

It quantifies the resistance that the system opposes to the passage of heat flux. Its expression depends on the considered geometry, k is the thermal conductivity and S is the surface of the layer.

In the same way, the stored energy in Joules by a mass m, having a mass capacity c_m at the temperature $T(K)$ is written:

$$U = \int Q dt = m c_m \Delta T \tag{14}$$

$$Q = m c_m \frac{dT}{dt} \tag{15}$$

Analogously, the equation of the intensity I which passes through a capacitance C_{elec} with a tension V is written:

$$I = C_{elec}\frac{dV}{dt} \tag{16}$$

The thermal capacity C (*J/K*) represents the storage of the heat in the layer of the wall and it is given by:

$$C = \rho c_m e_w S \tag{17}$$

The notion of thermal resistance allows the modelling of other phenomena, for example, the convective exchanges between a solid wall of temperature T_w and a fluid at a temperature T . Indeed, through Newton's law expressed in Eq. (18), a convective resistance R_{con} is defined by Eq. (19).

$$\left(T_w - T\right) = R_{conv} Q_{conv} \tag{18}$$

$$R_{conv} = \frac{1}{h_{conv} S} \tag{19}$$

Q_{con} is the convection heat flux and h_{con} is the convective exchange coefficient between the wall and the fluid.

The thermal/electrical equivalence makes it possible to derive the following properties:

- An imposed temperature is identical to a voltage generator.
- A heat flow is identical to an electric power generator.
- A body of mass m and heat capacity c_m; heated to the temperature T , is identical to a capacitor having a capacity mc_m related to the mass and the imposed voltage source.

5.2. *Physical module decomposition*

The passage from a purely thermal system to a model based on electrical phenomena requires an understanding of the physics that governs the system. In our configuration, there are 3 parts: concrete, phase change material and air tube. The study of the symmetry of the concrete block, in a wall or as an isolated element, allows us to adopt the decomposition of the system into 6 identical elements as represented in (Fig. 7).

Fig. 7. System decomposition into unitary elements.

Similarly, as a precaution, a study was conducted for the validation of the chosen geometric layout. Numerical simulations based on the finite element model were carried out in the case without ventilation.

Fig. 8 represents comparative study between 2D and 3D (configurations (b) and (c)) simulations of the lateral surface temperatures of the complete system and the unit element as well as the experimental data. (1) Configuration (a) illustrates a section of the unitary element at horizontal level on the tube. (2) Configuration (b) represents 3D unit element. (3) Configuration (c) shows the 3D complete system. It reveals that numerical results obtained from the 3D configurations are close to the experimental test then that obtained from 2D configuration. This is can be explained by the effect of the rib of the neglected concrete in the geometry (a). In addition, finite element flow modelling with geometry (a) is complicated to transform the outflow into an exchange coefficient. Therefore, configurations (b) and (c) can be considered to perform numerical validation. The configuration (c) has been adopted.

Fig. 8. Evolution of the average temperature on the inner surface for different geometric approaches in the case without ventilation.

According to the analysis carried out, the physical problem to be modelled is presented in Fig. 9; the diagram represents the chosen revealing zone. Physically, the influence of the tube is done in three dimensions. The RC circuit approach is based on the average temperatures of each modelled block; the horizontal flow between the two faces represents the main heat exchange in our system, the integration of ventilation adds a second exchange on the vertical. The modelling of these two exchanges with the electrical analogy requires a good understanding of the system from the two geometries (a) and (b) (Fig. 8). Thus, the hypothesis of a unidirectional transfer allows distinguishing three parallel levels that represent the succession of the elements constituting each part.

Fig. 9. The configuration of the revealing zone studied according to thermal exchanges.

5.3. *System modelling*

The RC circuit modelling, proposed in this work, is based on the use of the Matlab Simscape tool. Its library proposes several models for the direct integration of electrical, thermal, mechanical and hydraulic phenomena which allow to quickly creating physical system models in the Simulink environment.

The electrical model enables the creation of the circuit from the physical connections to obtain block diagrams. In the sense of electrical and thermal analogy, every part of our physical model will be replaced by an electrical circuit of resistances and capacitances, as well as for imposed boundary conditions.

Before arriving at the equivalent diagram representing the studied element, simple models were used to translate the behaviour of a single block of PCM. Thereafter, the other

elements were added progressively; the concrete parts as well as the air tube. The diagram in Fig. 10 represents the equivalent thermal model with its boundary conditions.

Fig. 10. Equivalent system diagram with the boundary conditions.

In our model, each concrete element would be replaced by an electrical circuit consisting of a resistance R_c and a capacitance C_c. According to the dimensions of each block, the formulas used in the calculation are:

$$R_c = \frac{e_c}{k_c S_c} \tag{20}$$

and

$$C_c = \rho_c c_{p_c} e_c S \tag{21}$$

with k_c, ρ_c and c_{p_c} are respectively, the characteristics of the concrete, the thermal conductivity, the density and the mass capacity, e_c and S_c represents the thickness and surface area of each part of the concrete.

In the experimental module, the lateral surface is subjected to convective exchanges; the convection coefficient h_{con} is calculated in the like in section 4. The convection resistance with the ambient air is written as follows:

$$R_{conv} = \frac{1}{h_{conv} S} \tag{22}$$

For taking into account the heat transfer by radiation from a surface to inside a building, there are several methods that estimate, in a more or less approximate way, the radiative exchanges between the surfaces. A linear equation expressing the heat flux between a wall of temperature T and all the other walls is used [52]. The radiative heat flux on the lateral face is given by:

$$Q_{rad} = h_{rad} S (T - T_w) \tag{23}$$

The expression of h_{rad} depends on the average temperature of the walls T_w. This temperature is considered equal to the ambient temperature:

$$h_{rad} = 4 \varepsilon \sigma T_{amb}^{3} \tag{24}$$

The radiative resistance R_{rad} on the lateral surface of our model is:

$$R_{rad} = \frac{1}{h_{rad} S} \tag{25}$$

503 The elements containing the paraffin/polymer mixture constitute a system that stores the
504 heat in a sensible and latent form, which results in a storage capacity and a thermal
505 resistance that vary according to the solid and liquid state of the mixture. This is why in
506 order to encompass the entire phenomenon of phase change by electrical analogy; each
507 volume of PCM is replaced by an electrical block consisting of a resistance and a variable
508 capacity depending on the temperature.

509 The variable capacity C_{pcn} for a PCM block having a volume V_{pcm} is given by Eq. (26).

510 $$C_{pcm} = \rho_{pcm}\, c_{p\,pcm}\, V_{pcm} \tag{26}$$

511 with $c_{p\,pcm}$ is the variation of specific capacity of the mixture adopted for thermo-electric
512 modelling.

513 The density of the phase change material is defined by Eq. (27).

514 $$\rho_{pcm} = \begin{cases} \rho_s & ;\ T < T_{om} \\ \dfrac{(\rho_s + \rho_l)}{2} & ;\ T_{om} \le T \le T_{sl} \\ \rho_l & ;\ T > T_{sl} \end{cases} \tag{27}$$

515 where T_{om} is the temperature that marks the start of the fusion obtained from the DSC
516 experimental measurements and T_{sl} is the solid-liquid phase transition temperature.

517 The specific capacity modelling is based on the experimentally obtained curve, the work of
518 Alisetti and Roy [53] shows that the equivalent function shape $c_{p\,eq}(T)$ has only a low
519 influence on heat transfer. Taking into account the phase change in the transition interval
520 which is defined by:

521 • The melting temperature T_{sl}
522 • The melting interval ΔT determined from the melting curve obtained by DSC
523 (first initiation of the phase change T_{om} to the peak of transition)
524 • The calculated latent heat (integration of the total surface during the solid-
525 liquid transition)
526 • Specific heats in the solid and liquid state (c_{p_s} and c_{p_l})

527 **Fig. 11.** Adopted modelling of the specific capacity of the PCM.

528 The adopted equivalent thermal capacity is, as simple as possible according to the
529 announced indications; it respects the conservation of the amount of involved energy. Fig.
530 11 shows the evolution of the involved thermal capacity; its equation is written as:

$$c_{p_{pcm}} = \begin{cases} c_{p_s} & ;\ T < T_{om} \\ c_{p_{eq}} = \dfrac{\Delta L}{T_{sl} - T_{om}} & ;\ T_{om} \le T \le T_{sl} \\ c_{p_l} & ;\ T > T_{sl} \end{cases} \quad (28)$$

Likewise, as given in relation (29), the resistance of each block of the PCM is a variable resistance depending on the liquid or solid conductivity according to the temperature:

$$R_{pcm} = \frac{e_{pcm}}{k_{pcm} S_{pcm}} \quad (29)$$

where e_{pcm} is the thickness of each part of the PCM and k_{pcm} is the variable conductivity according to the state of the PCM solution which is expressed by Eq. (30).

$$k_{pcm} = \begin{cases} k_s & ;\ T < T_{om} \\ (k_s + k_l)/2 & ;\ T_{om} \le T \le T_{sl} \\ k_l & ;\ T > T_{sl} \end{cases} \quad (30)$$

- *Tube and airflow*

Taking into account the tube in the modelling of the studied thermal system begins with its thermal resistance. The assumption of a unidirectional heat transfer and the behaviour of the module impose the consideration of two heat flows which exchange to the right and to the left of the tube. Subsequently, splitting the thermal resistance in half is necessary to differentiate the total resistance on each side.

The thermal resistance of the tube R_t is written as:

$$R_t = \frac{\log\left(\dfrac{D_o}{D_i}\right)}{2\pi k_t L_t} \quad (31)$$

where D_i and D_o are the inner and outer diameters of the tube, L_t is the length of the tube and k_t is the thermal conductivity of the tube. The modelling of the flow is different according to the state of the tubes: open or ventilated. The dimensions of the tube do not allow the appearance of a significant convective mode in the open configuration case. The air part through the tube is modelled with a thermal resistance of heat conduction expressed by Eq. (32).

$$R_{air} = \frac{D_i}{k_{air} S_{air}} \quad (32)$$

where k_{air} is the thermal conductivity of the air and S_{ai} is the lateral surface of the air volume.

In the case of forced flow with fans, the problem evolves in the three directions; taking into account the passage of air using the exchange coefficients is not sufficient for modelling electrical-thermal equivalence. The injection of air through the tube is characterized by two elements, the speed and the temperature of the incoming air. In the sense of electrical analogy modelling, a temperature or a voltage will model the interaction of the flow of air entering with the flows exchanged horizontally across the system.

In order to identify this temperature, it is necessary to express the heat balance equation at the midpoint of the tube which is the mean temperature over the height. Fig. 12(a) describes the flows exchanged in the horizontal and vertical direction.

Fig. 12. Airflow modelling through the tube: **(a)** The schematic diagram of modelling parameters, **(b)** Equivalent electrical diagram of the middle part containing the tube.

The heat balance equation (33) can be written and then resolved for the air temperature in the middle of the system T_{air}:

$$\dot{m}_{air} C_{p_{air}} (T_{in} - T_{out}) = R_{T1}(T_f - T_{air}) + R_{T2}(T_{amb} - T_{air}) \tag{33}$$

where R_{T1} and R_{T2} represent the total thermal resistance respectively on the left between T_{wo} and T_{air}, and on the right between T_{air} and T_{aml}. T_{in} and T_{out} are respectively the inlet and outlet air temperature across the tube.

The resolution of the air temperature, as a function of the travelled distance, in the case where the convection coefficients through the tube are equal [54], gives the expression (34).

$$T_{air} = \frac{H_1 T_{wo} + H_2 T_{amb}}{H_1 + H_2} + \exp\left(\frac{-(H_1 + H_2)S}{\dot{m}_{air} C_{p_{air}}}\right)\left(T_{in} - \frac{H_1 T_{wo} + H_2 T_{amb}}{H_1 + H_2}\right) \tag{34}$$

with

$$H_1 = \left(\frac{e_c}{k_c} + \frac{e_{pcm}}{k_{pcm}} + D_o \frac{\log(D_o / D_i)}{4\pi k_t} + \frac{1}{h_v}\right)^{-1} \tag{35}$$

$$H_2 = \left(H_1^{-1} + (h_{rad} + h_{conv})^{-1}\right)^{-1} \tag{36}$$

where H_1 and H_2 are two coefficients that translate the heat transfer by convection and conduction on both sides of the tube. Thus, h_v, h_{rad} and h_{con} are respectively the coefficient of convection through the tube during ventilation, the coefficient of radiation on

580 the lateral surface and the convection coefficient with the ambient air. These coefficients are
581 calculated previously in the description of the models.

582 The expression of the temperature T_{air} depends on the ambient temperature T_{aml} and the
583 temperature T_{wo} that simulates the thermal solicitations on the lateral surface. When
584 integrated into the RC model, this temperature is equivalent to a variable voltage generator
585 according to the temperature of the PCM which reflects the variations of the resistances
586 expressed in the coefficients H_1 and H_2.

587 Fig. 12(b) shows the equivalent electrical diagram used in the middle part of the model (see
588 Fig. 10). The arrows on the components indicate that these elements are variable; it
589 concerns the parts of the PCM as well as the temperature used in the modelling of the
590 airflow. In the RC model thus developed, the objective was to evaluate the response of the
591 surface of the system; a 1R1C circuit was used to model each part. The spatial discretization
592 used is fine enough to accurately determine the temperature of the output surfaces. If the
593 objective is to follow the detailed evolution of the temperature in a specific material, a
594 discretization with more nodes will be applied to each element [55].

595 **6. Validation results and discussion**

596 Fig. 13 presents the comparison between the results obtained from the FEM/RC simulations
597 and those obtained by experimentation for the two cases without and with ventilation. The
598 FEM was developed primarily as a reference for examining the accuracy of the model with
599 RC network. For this purpose, the first comparison concerns the results of the FEM with the
600 experiment; Table 2 represents the values of the relative errors calculated with respect to
601 the experimental data. The average relative error does not exceed 1.4% and the maximum
602 relative error is about 4.6% in the case without ventilation. This small discrepancy between
603 these data is probably due to three factors: the degree of uniformity of the thermal power
604 given by the heating resistor, the influence of thermal insulation, which is not ideal for
605 eliminating all heat losses. For modelling the PCM, the used effective thermal capacity, only
606 involves the measurement performed during the fusion.

607 Indeed, during solidification, the curve is slightly different. Taking into account this
608 hysteresis between fusion and solidification during numerical validation has been the subject
609 of numerous studies. Baghban et al. [56] indicated that it is essential to use the melting and
610 freezing characteristics of PCM to achieve good agreement between experimental and
611 numerical results. Kośny [57] stated that the use of simplified algorithms that do not include
612 hysteresis can lead to significant inaccuracies for a large number of non-paraffinic organic
613 and inorganic PCMs. Goia et al. [58] demonstrated that for paraffin organic PCM, the
614 available building energy simulation software is fairly accurate even if the effect of hysteresis
615 is neglected.

Thus, according to these different studies, the fact that hysteresis is not taken into account does not affect significantly our results. Despite the noted slight difference, there is a good agreement between the simulation and the experiment, which makes possible to validate the finite element model used in the simulation.

Fig. 13. Temperature of the surface of the concrete block, comparison of the experimental data with the two models RC and FEM: **(a)** without ventilation, **(b)** with ventilation.

For comparison of the RC model with the experimental data, Fig. 13 illustrates a similar trend of variation between the simulated and measured values, in both cases with and without ventilation. Relative errors calculated with respect to the experiment are acceptable for direct validation. The difference between the two numerical models is mainly due to the modelling of the phenomenon of phase change with the electrical analogy which is based on the use of variable resistances and capacitances. Thus, the simplifying assumptions used in the RC model do not allow capturing the simulated complexity in 3D with the CFD model. These discrepancies have no significant effect on the accuracy of the obtained simulation results. The temperature on the lateral surface of the system is very well predicted by the RC network model and the maximum relative error is less than 4.0%. It can be concluded that the developed RC model can be directly used to replace a fairly heavy CFD simulation in computing time.

Table 2. Results of relative error between experimental and numerical data.

Following the analysis previously conducted on the experimental results, Fig. 13(b) clearly illustrates that ventilation occurs in the heat transfer and that its influence even acts on the heated side surface. The temperature evolution of this face gives more information on the state of the PCM inside. For both cases, a surface can be distinguished, which evolves between the horizontal line that shows the phase change temperature of the mixture T_{sl} and the ambient temperature T_{amb}. The temperature variation on the internal face evolves in this surface; it approaches of T_{sl} in the case without ventilation and tends towards T_{amb} with ventilation.

In order to make a link against a real situation, this difference with respect to the ambient temperature defines the heat flux passing through the wall and consequently the energy requirement of air conditioning to reach the comfort temperature replaced here by the ambient temperature. The gradient of the applied thermal heat flux acts progressively, the concrete part rapidly reaches the steady state and all the energy transmitted is stored by PCM. Gradually, the temperature of the internal face exceeds the ambient temperature and a heat flux begins to leave this face towards the ambient environment. After stopping the thermal solicitations, the temperature decreases and the PCM become a source that releases energy. In Fig. 13(a), the stabilization bearing below T_{sl} marks the solidification with a temperature close and parallel to T_{sl}. The air injection at T_{amb} by ventilation after stopping of the thermal power gives rise to a vertical heat transfer which is added to that

established horizontally. The presence of the insulation on the heated side explains that the descent, noted on the heating curve is mainly due to the evacuation of energy through the tubes (Fig. 13(b)), the influence is significant because the average temperature on the internal face goes from 25 to 23.8 °C. Thus, decreasing the energy requirement is also accompanied by a significant capacity to increase the temperature of the air entering through the tubes.

7. Conclusions

In this work, a study of a thermal system developed to regulate the indoor temperature of a building have been proposed. The combination of the inertia effect of PCM introduced in the wall elements coupled to a ventilation system leads to a better use of the energy stored in a building wall. This solution uses building materials as a basic element and aims to improve the thermal response of PCM building walls and to demonstrate the feasibility of such an energy solution.

An experimental device was made based on a hollow concrete block filled with mechanically stable paraffin and equipped with ventilation tubes. The results have confirmed that the insertion of paraffin with tubes allows the creation of a thermal phase shift and the improvement of the inertial capabilities of the studied element. The ventilated tubes play the role of the regulator to unload the system and thus heat the injected air. The operation principle of this type of system is confirmed. However, the small scale of the experiment and the influence of the air flow at the entry of the tubes constitute limitations for the generalization of the experimental results in the real scale of a wall. In this framework, it is important to specify that there are many optimization parameters that can be used to operate the system at the wall scale as well as adaptation to climate conditions and desired operation. These parameters are: tube dimensions compared to the amount of PCM, flow velocity, the geometry of the tubes and their arrangement in the cavities, the phase change temperature as well as the type of the PCM and the materials of the constructions used.

On the numerical section, an RC network model has been developed, it proposes a simplified approach to models the thermal heat transfer by using the Simscape tool under Matlab, it allows both to get closer to the performance of CFD models in taking into account the evolution of the physical phenomena and it offers a great speed of the execution of the simulations, a parameter required in the calculations related to the building. Similarly, the model proposes a new approach to modelling the phase change by using grey boxes with their resistances and varying capacitances. The finite element model is proposed as a reference for comparing the accuracy of the RC model.

The analysis of the obtained results has confirmed the validity of the RC model for predicting the temperature evolutions of the system surface. The model developed in this study will be used to define the quantity of the PCM and the optimal dimensions of the elements of the system according to scenarios closer to reality. This study has made possible to test the

692 feasibility and the performance of this proposed solution, and the validation of numerical
693 tools allows the passage from elementary reasoning to a larger scale, this will be the basis
694 for achieving the final aim of obtaining an optimal wall based on PCM filled elements and
695 controlled by ventilation pipes.

Acknowledgements

The authors would like to thank the Grand Troyes Community in France for partially funding this work. The LMT/ENS-Paris Saclay for affording the first version set-up.

References

[1] D. Zhou, C.Y. Zhao, Y. Tian, Review on thermal energy storage with phase change materials (PCMs) in building applications, Appl. Energy. 92 (2012) 593–605. doi:10.1016/j.apenergy.2011.08.025.

[2] A.M. Khudhair, M.M. Farid, A review on energy conservation in building applications with thermal storage by latent heat using phase change materials, Energy Convers. Manag. 45 (2004) 263–275. doi:10.1016/S0196-8904(03)00131-6.

[3] F. Kuznik, D. David, K. Johannes, J.J. Roux, A review on phase change materials integrated in building walls, Renew. Sustain. Energy Rev. 15 (2011) 379–391. doi:10.1016/j.rser.2010.08.019.

[4] L.F. Cabeza, A. Castell, C. Barreneche, A. De Gracia, A.I. Fernández, Materials used as PCM in thermal energy storage in buildings: A review, Renew. Sustain. Energy Rev. 15 (2011) 1675–1695. doi:10.1016/j.rser.2010.11.018.

[5] L. Royon, L. Karim, A. Bontemps, Thermal energy storage and release of a new component with PCM for integration in floors for thermal management of buildings, Energy Build. 63 (2013) 29–35. doi:10.1016/j.enbuild.2013.03.042.

[6] L. Royon, L. Karim, A. Bontemps, Optimization of PCM embedded in a floor panel developed for thermal management of the lightweight envelope of buildings, Energy Build. 82 (2014) 385–390. doi:10.1016/j.enbuild.2014.07.012.

[7] E.M. Alawadhi, Thermal analysis of a building brick containing phase change material, Energy Build. 40 (2008) 351–357. doi:10.1016/j.enbuild.2007.03.001.

[8] K. Lin, Y. Zhang, X. Xu, H. Di, R. Yang, P. Qin, Modeling and simulation of under-floor electric heating system with shape-stabilized PCM plates, Build. Environ. 39 (2004) 1427–1434. doi:10.1016/j.buildenv.2004.04.005.

[9] R. Ansuini, R. Larghetti, A. Giretti, M. Lemma, Radiant floors integrated with PCM for indoor temperature control, Energy Build. 43 (2011) 3019–3026. doi:10.1016/j.enbuild.2011.07.018.

[10] A. Figueiredo, J. Lapa, R. Vicente, C. Cardoso, Mechanical and thermal characterization of concrete with incorporation of microencapsulated PCM for applications in thermally activated slabs, Constr. Build. Mater. 112 (2016) 639–647. doi:10.1016/j.conbuildmat.2016.02.225.

[11] A. Castell, I. Martorell, M. Medrano, G. Pérez, L.F. Cabeza, Experimental study of using PCM in brick constructive solutions for passive cooling, Energy Build. 42 (2010) 534–

540. doi:10.1016/j.enbuild.2009.10.022.

[12] L.F. Cabeza, C. Castellón, M. Nogués, M. Medrano, R. Leppers, O. Zubillaga, Use of microencapsulated PCM in concrete walls for energy savings, Energy Build. 39 (2007) 113–119. doi:10.1016/j.enbuild.2006.03.030.

[13] M. Zhang, M.A. Medina, J.B. King, Development of a thermally enhanced frame wall with phase-change materials for on-peak air conditioning demand reduction and energy savings in residential buildings, Int. J. Energy Res. 29 (2005) 795–809. doi:10.1002/er.1082.

[14] C. Zhang, Y. Chen, L. Wu, M. Shi, Thermal response of brick wall filled with phase change materials (PCM) under fluctuating outdoor temperatures, Energy Build. 43 (2011) 3514–3520. doi:10.1016/j.enbuild.2011.09.028.

[15] P. Principi, R. Fioretti, Thermal analysis of the application of PCM and low emissivity coating in hollow bricks, Energy Build. 51 (2012) 131–142. doi:10.1016/j.enbuild.2012.04.022.

[16] X. Wang, H. Yu, L. Li, M. Zhao, Experimental assessment on the use of phase change materials (PCMs)-bricks in the exterior wall of a full-scale room, Energy Convers. Manag. 120 (2016) 81–89. doi:10.1016/j.enconman.2016.04.065.

[17] A. Pasupathy, L. Athanasius, R. Velraj, R. V. Seeniraj, Experimental investigation and numerical simulation analysis on the thermal performance of a building roof incorporating phase change material (PCM) for thermal management, Appl. Therm. Eng. 28 (2008) 556–565. doi:10.1016/j.applthermaleng.2007.04.016.

[18] H. Elarga, S. Fantucci, V. Serra, R. Zecchin, E. Benini, Experimental and numerical analyses on thermal performance of different typologies of PCMs integrated in the roof space, Energy Build. 150 (2017) 546–557. doi:10.1016/j.enbuild.2017.06.038.

[19] S. Guichard, F. Miranville, D. Bigot, H. Boyer, A thermal model for phase change materials in a building roof for a tropical and humid climate: Model description and elements of validation, Energy Build. 70 (2014) 71–80. doi:10.1016/j.enbuild.2013.11.079.

[20] F. Goia, M. Perino, V. Serra, Improving thermal comfort conditions by means of PCM glazing systems, Energy Build. 60 (2013) 442–452. doi:10.1016/j.enbuild.2013.01.029.

[21] D. Li, Y. Wu, C. Liu, G. Zhang, M. Arıcı, Energy investigation of glazed windows containing Nano-PCM in different seasons, Energy Convers. Manag. 172 (2018) 119–128. doi:10.1016/j.enconman.2018.07.015.

[22] S. Li, K. Zou, G. Sun, X. Zhang, Simulation research on the dynamic thermal performance of a novel triple-glazed window filled with PCM, Sustain. Cities Soc. 40 (2018) 266–273. doi:10.1016/j.scs.2018.01.020.

[23] E.M. Alawadhi, Using phase change materials in window shutter to reduce the solar heat gain, Energy Build. 47 (2011) 421–429. doi:10.1016/j.enbuild.2011.12.009.

771 [24] K.A.R. Ismail, J. Henriquez, Thermally effective windows with moving phase change
772 material curtains, Appl. Therm. Eng. 21 (2001) 1909–1923. doi:10.1016/S1359-
773 4311(01)00058-8.

774 [25] A. Komerska, L. Bianco, V. Serra, S. Fantucci, M. Rosiński, Experimental analysis of an
775 external dynamic solar shading integrating PCMs: First results, in: Energy Procedia,
776 2015: pp. 3452–3457. doi:10.1016/j.egypro.2015.11.125.

777 [26] K. Nagano, S. Takeda, T. Mochida, K. Shimakura, T. Nakamura, Study of a floor supply
778 air conditioning system using granular phase change material to augment building
779 mass thermal storage—Heat response in small scale experiments, Energy Build. 38
780 (2006) 436–446. doi:10.1016/j.enbuild.2005.07.010.

781 [27] A. Waqas, Z. Ud Din, Phase change material (PCM) storage for free cooling of buildings
782 - A review, Renew. Sustain. Energy Rev. 18 (2013) 607–625.
783 doi:10.1016/j.rser.2012.10.034.

784 [28] M. Iten, S. Liu, A. Shukla, A review on the air-PCM-TES application for free cooling and
785 heating in the buildings, Renew. Sustain. Energy Rev. 61 (2016) 175–186.
786 doi:10.1016/j.rser.2016.03.007.

787 [29] H. Akeiber, P. Nejat, M.Z.A. Majid, M.A. Wahid, F. Jomehzadeh, I. Zeynali Famileh, J.K.
788 Calautit, B.R. Hughes, S.A. Zaki, A review on phase change material (PCM) for
789 sustainable passive cooling in building envelopes, Renew. Sustain. Energy Rev. 60
790 (2016) 1470–1497. doi:10.1016/j.rser.2016.03.036.

791 [30] M. Ahmad, A. Bontemps, H. Sallée, D. Quenard, Experimental investigation and
792 computer simulation of thermal behaviour of wallboards containing a phase change
793 material, Energy Build. 38 (2006) 357–366. doi:10.1016/j.enbuild.2005.07.008.

794 [31] F. Kuznik, J. Virgone, Experimental investigation of wallboard containing phase change
795 material: Data for validation of numerical modeling, Energy Build. 41 (2009) 561–570.
796 doi:10.1016/j.enbuild.2008.11.022.

797 [32] C. Hasse, M. Grenet, A. Bontemps, R. Dendievel, H. Sallée, Realization, test and
798 modelling of honeycomb wallboards containing a Phase Change Material, Energy
799 Build. 43 (2011) 232–238. doi:10.1016/j.enbuild.2010.09.017.

800 [33] D. Zhang, Z. Li, J. Zhou, K. Wu, Development of thermal energy storage concrete, Cem.
801 Concr. Res. 34 (2004) 927–934. doi:10.1016/j.cemconres.2003.10.022.

802 [34] T. Lee, D.. Hawes, D. Banu, D. Feldman, Control aspects of latent heat storage and
803 recovery in concrete, Sol. Energy Mater. Sol. Cells. 62 (2000) 217–237.
804 doi:10.1016/S0927-0248(99)00128-2.

805 [35] K. Kant, A. Shukla, A. Sharma, Heat transfer studies of building brick containing phase
806 change materials, Sol. Energy. 155 (2017) 1233–1242.
807 doi:10.1016/j.solener.2017.07.072.

808 [36] Y. Zhang, G. Zhou, K. Lin, Q. Zhang, H. Di, Application of latent heat thermal energy
809 storage in buildings: State-of-the-art and outlook, Build. Environ. 42 (2007) 2197–

2209. doi:10.1016/j.buildenv.2006.07.023.

[37] A. Foucquier, S. Robert, F. Suard, L. Stéphan, A. Jay, State of the art in building modelling and energy performances prediction: A review, Renew. Sustain. Energy Rev. 23 (2013) 272–288. doi:10.1016/j.rser.2013.03.004.

[38] M.G. Davies, Optimal RC networks for walls, Appl. Math. Model. 6 (1982) 403–404. doi:10.1016/S0307-904X(82)80108-X.

[39] S. Goyal, P. Barooah, A method for model-reduction of non-linear thermal dynamics of multi-zone buildings, Energy Build. 47 (2012) 332–340. doi:10.1016/j.enbuild.2011.12.005.

[40] G. Fraisse, C. Viardot, O. Lafabrie, G. Achard, Development of a simplified and accurate building model based on electrical analogy, Energy Build. 34 (2002) 1017–1031. doi:10.1016/S0378-7788(02)00019-1.

[41] J.H. Kämpf, D. Robinson, A simplified thermal model to support analysis of urban resource flows, Energy Build. 39 (2007) 445–453. doi:10.1016/j.enbuild.2006.09.002.

[42] H. Park, N. Martaj, M. Ruellan, R. Bennacer, E. Monmasson, Modeling of a building system and its parameter identification, J. Electr. Eng. Technol. 8 (2013) 975–983. doi:10.5370/JEET.2013.8.5.975.

[43] B. Bueno, L. Norford, G. Pigeon, R. Britter, A resistance-capacitance network model for the analysis of the interactions between the energy performance of buildings and the urban climate, Build. Environ. 54 (2012) 116–125. doi:10.1016/j.buildenv.2012.01.023.

[44] A. Laaouatni, N. Martaj, R. Bennacer, M. Elomari, M. El Ganaoui, Study of improving the thermal response of a construction material containing a phase change material, J. Phys. Conf. Ser. 745 (2016) 032131. doi:10.1088/1742-6596/745/3/032131.

[45] A. Laaouatni, N. Martaj, R. Bennacer, M. El Omari, M. El Ganaoui, Phase change materials for improving the building thermal inertia, Energy Procedia. 139 (2017) 744–749. doi:10.1016/j.egypro.2017.11.281.

[46] P. Lamberg, R. Lehtiniemi, A.-M. Henell, Numerical and experimental investigation of melting and freezing processes in phase change material storage, Int. J. Therm. Sci. 43 (2004) 277–287. doi:10.1016/j.ijthermalsci.2003.07.001.

[47] N.S. Dhaidan, J.M. Khodadadi, T.A. Al-Hattab, S.M. Al-Mashat, Experimental and numerical study of constrained melting of n-octadecane with CuO nanoparticle dispersions in a horizontal cylindrical capsule subjected to a constant heat flux, Int. J. Heat Mass Transf. 67 (2013) 523–534. doi:10.1016/j.ijheatmasstransfer.2013.08.001.

[48] S.N. AL-Saadi, Z. (John) Zhai, Modeling phase change materials embedded in building enclosure: A review, Renew. Sustain. Energy Rev. 21 (2013) 659–673. doi:10.1016/j.rser.2013.01.024.

[49] M. Ahmad, A. Bontemps, H. Sallée, D. Quenard, Thermal testing and numerical simulation of a prototype cell using light wallboards coupling vacuum isolation panels

and phase change material, Energy Build. 38 (2006) 673–681. doi:10.1016/j.enbuild.2005.11.002.

[50] W.H. McAdams, Heat Transmission, 3rd ed., McGraw-Hill, New York, 1954.

[51] F.P. Incropera, D.P. DeWitt, Fundamentals of heat and mass transfer, 3rd ed., Wiley, New York, 1990.

[52] M.G. Davies, Optimal designs for star circuits for radiant exchange in a room, Build. Environ. 18 (1983) 135–150. doi:10.1016/0360-1323(83)90006-9.

[53] E.L. Alisetti, S.K. Roy, Forced Convection Heat Transfer to Phase Change Material Slurries in Circular Ducts, J. Thermophys. Heat Transf. 14 (2000) 115–118. doi:10.2514/2.6499.

[54] V. Dermardiros, Y. Chen, A.K. Athienitis, Modelling of an active PCM thermal energy storage for control applications, Energy Procedia. 78 (2015) 1690–1695. doi:10.1016/j.egypro.2015.11.261.

[55] N. Stathopoulos, M. El Mankibi, R. Issoglio, P. Michel, F. Haghighat, Air-PCM heat exchanger for peak load management: Experimental and simulation, Sol. Energy. 132 (2016) 453–466. doi:10.1016/j.solener.2016.03.030.

[56] M.H. Baghban, P.J. Hovde, A. Gustavsen, Numerical Simulation of a Building Envelope with High Performance Materials, COMSOL Conf. 2010 Paris. (2010) 1–5. https://www.comsol.se/paper/download/63393/baghban_paper.pdf (accessed September 6, 2018).

[57] J. Kośny, PCM-Enhanced Building Components, Springer International Publishing, 2015. doi:10.1007/978-3-319-14286-9.

[58] F. Goia, G. Chaudhary, S. Fantucci, Modelling and experimental validation of an algorithm for simulation of hysteresis effects in phase change materials for building components, Energy Build. 174 (2018) 54–67. doi:10.1016/j.enbuild.2018.06.001.

	Density ρ (kg/m^3)	Thermal conductivity λ (W/(m K))	Specific heat capacity C_p (J/(kg K))
PCM T < 27.5 °C T > 27.5 °C	 850 780	 0.28 0.18	 2800 2500
concrete (at T=25 °C)	1000	0.9	1000
PVC	1400	0.16	1046

Table 1. Thermo-physical properties of the materials constituting the system.

		Relative error (average) (%)	Relative error (maximum) (%)
without ventilation	RC-model	1.32	2.61
	FEM	1.14	4.58
with ventilation	RC-model	1.37	3.38
	FEM	1.32	3.03

Table 2. Results of relative error between experimental and numerical data.

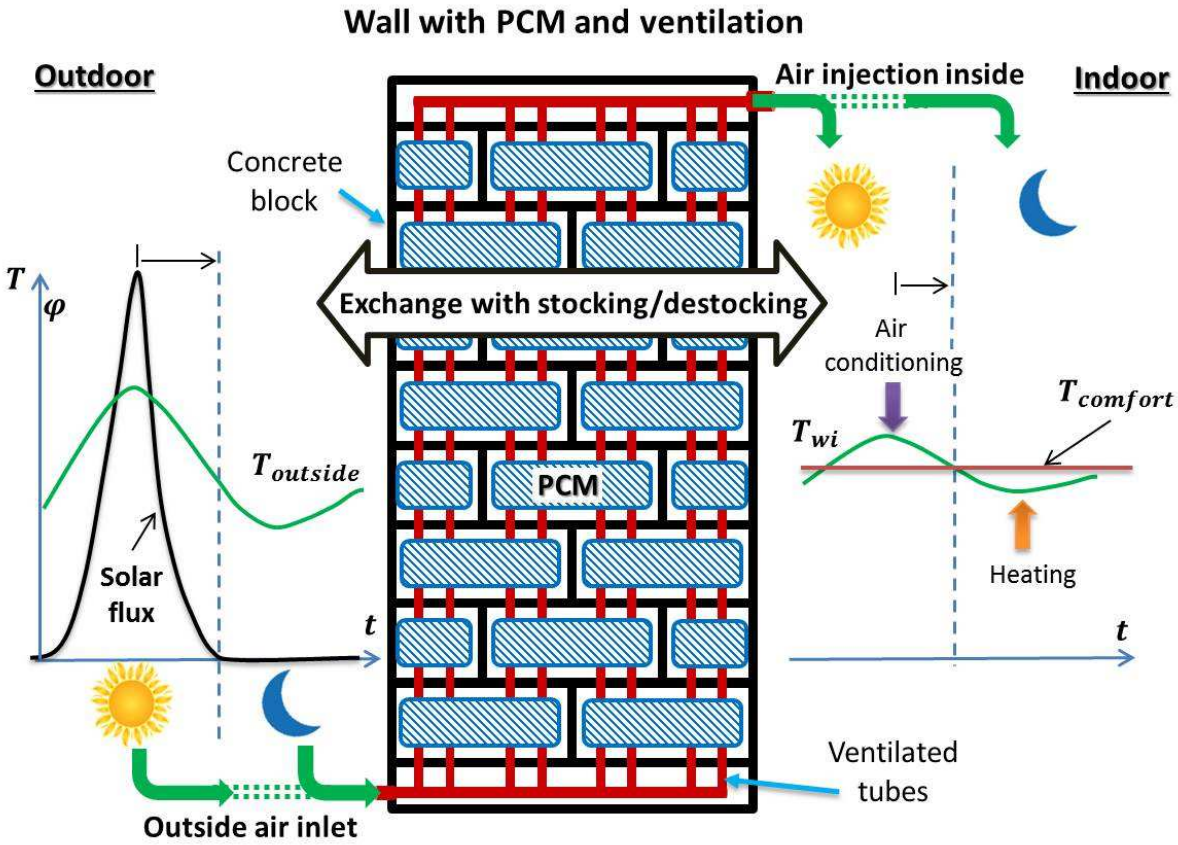

Fig. 1. Principle and utility of the tubes in the developed solution.

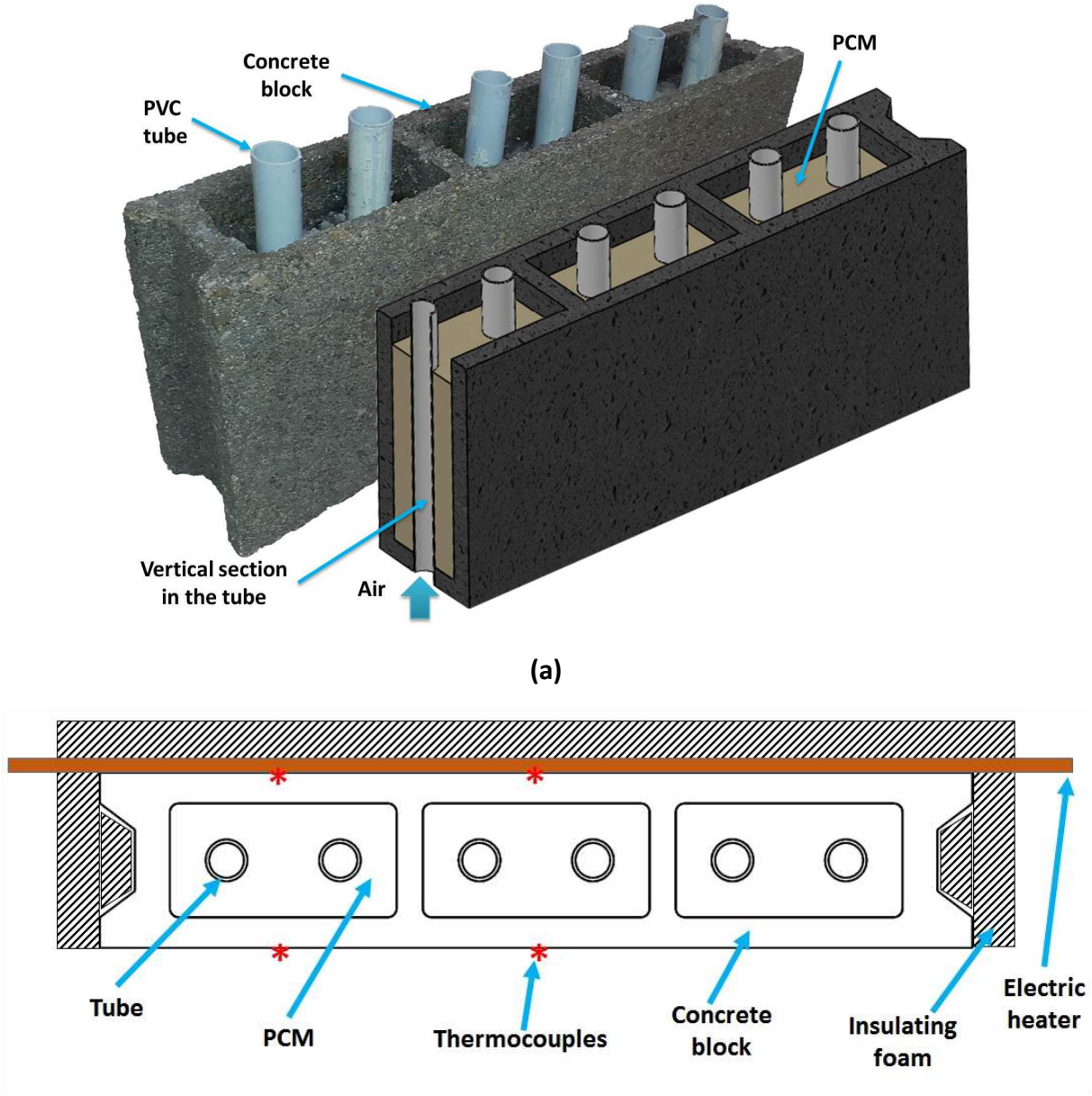

Fig. 2. Description of the developed system: **(a)** Schematic of the ventilated hollow concrete block integrating PCM **(b)** Schematic diagram of the experimental setup.

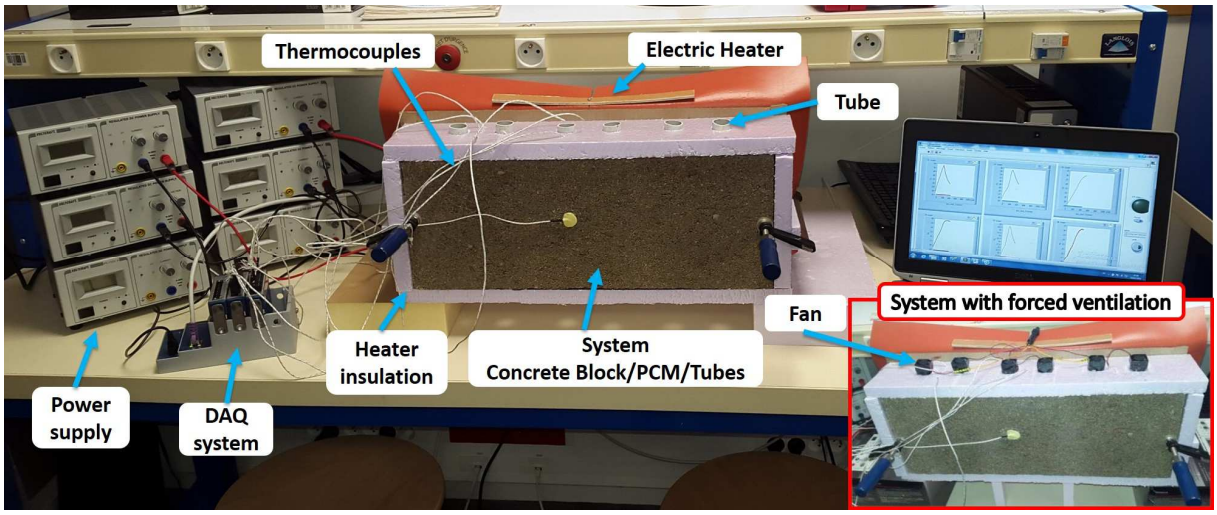

Fig. 3. Photography of the experimental bench.

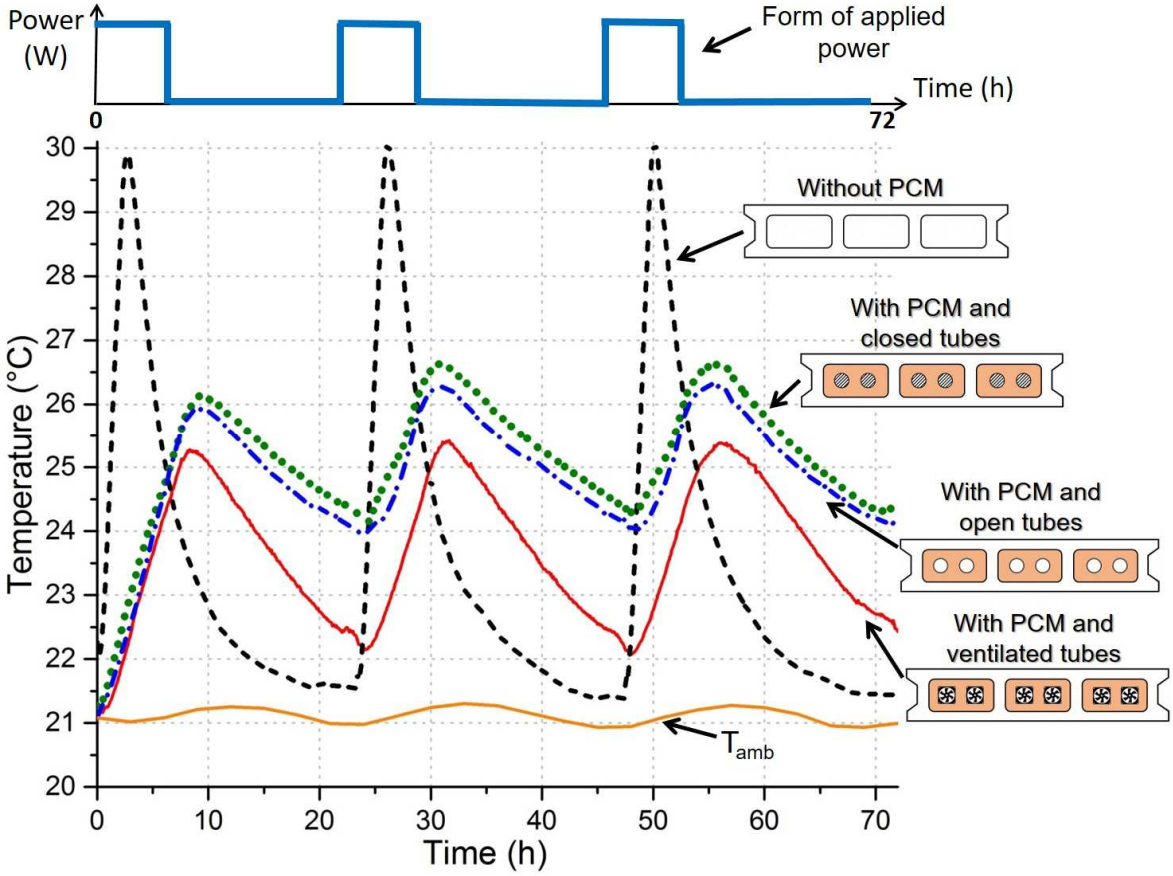

Fig. 4. Evolution of the temperature on the lateral surface of the concrete block for different configurations.

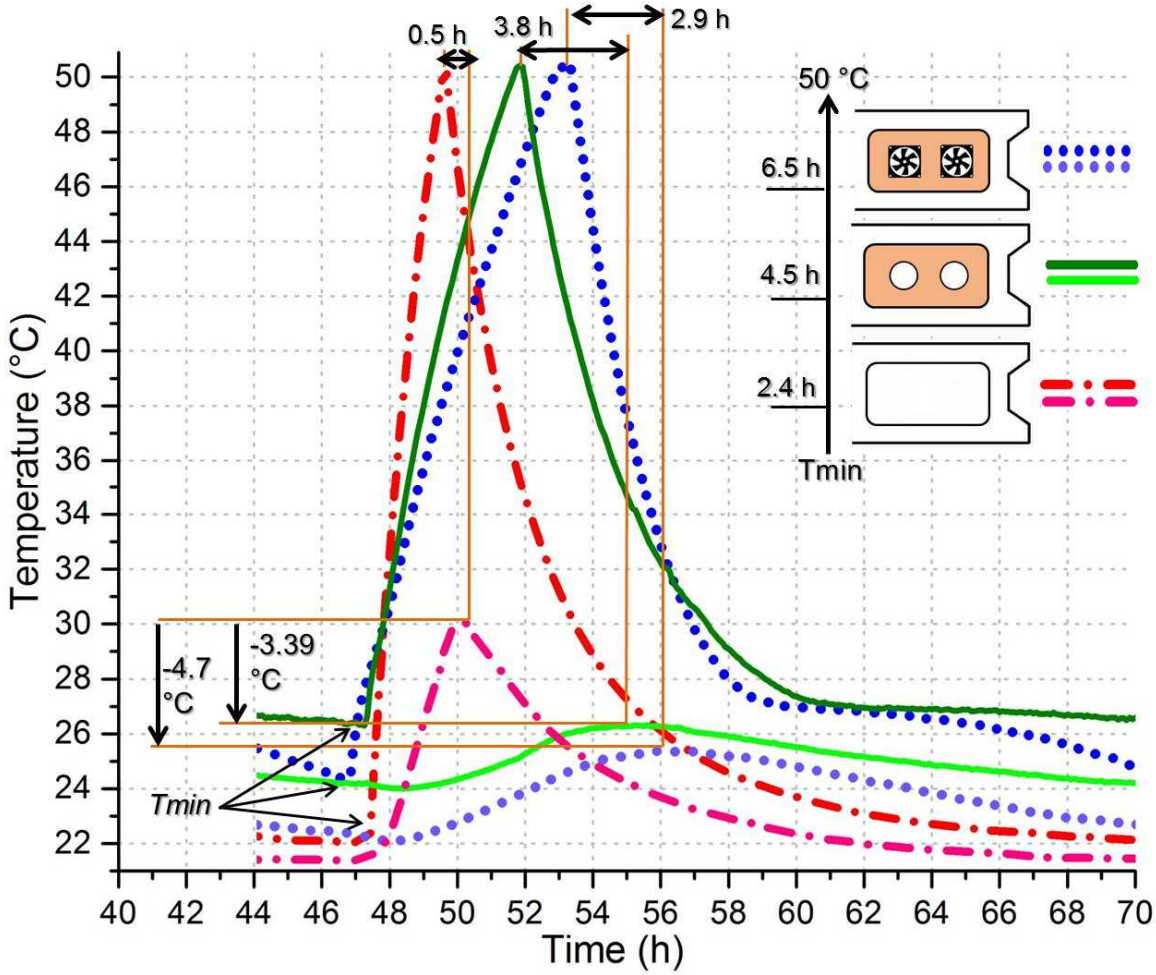

Fig. 5. Temperature analysis on the lateral surface of the concrete block for the different configurations starting from the third cycle.

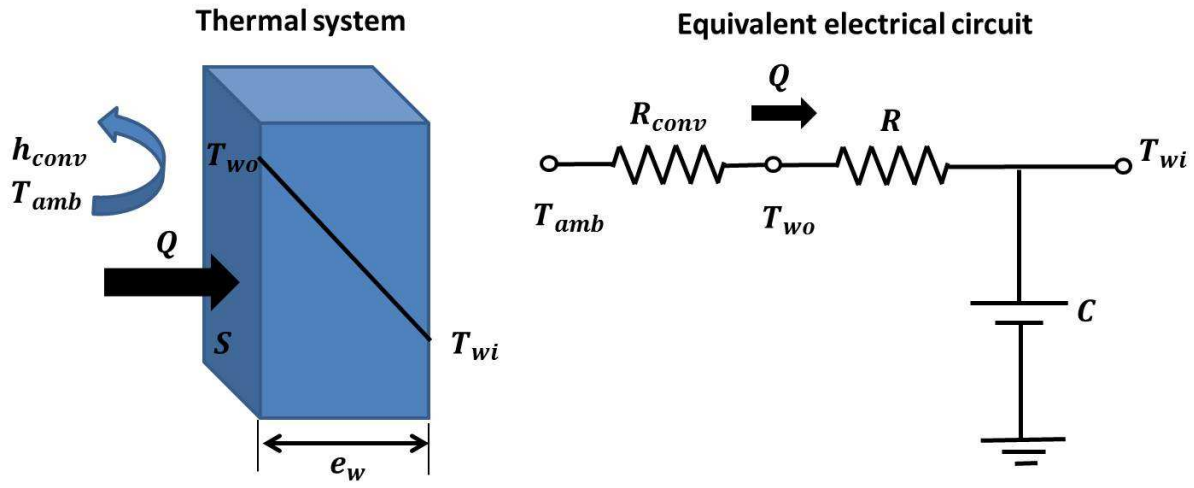

Fig. 6. Equivalent electrical circuit (1R1C) in the unsteady case.

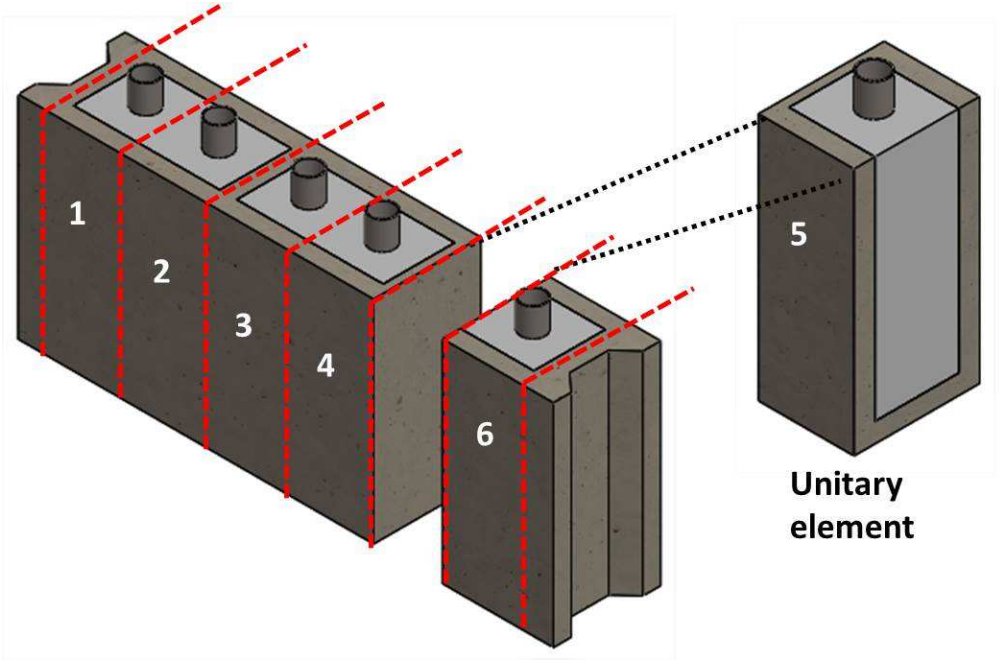

Fig. 7. System decomposition into unitary elements.

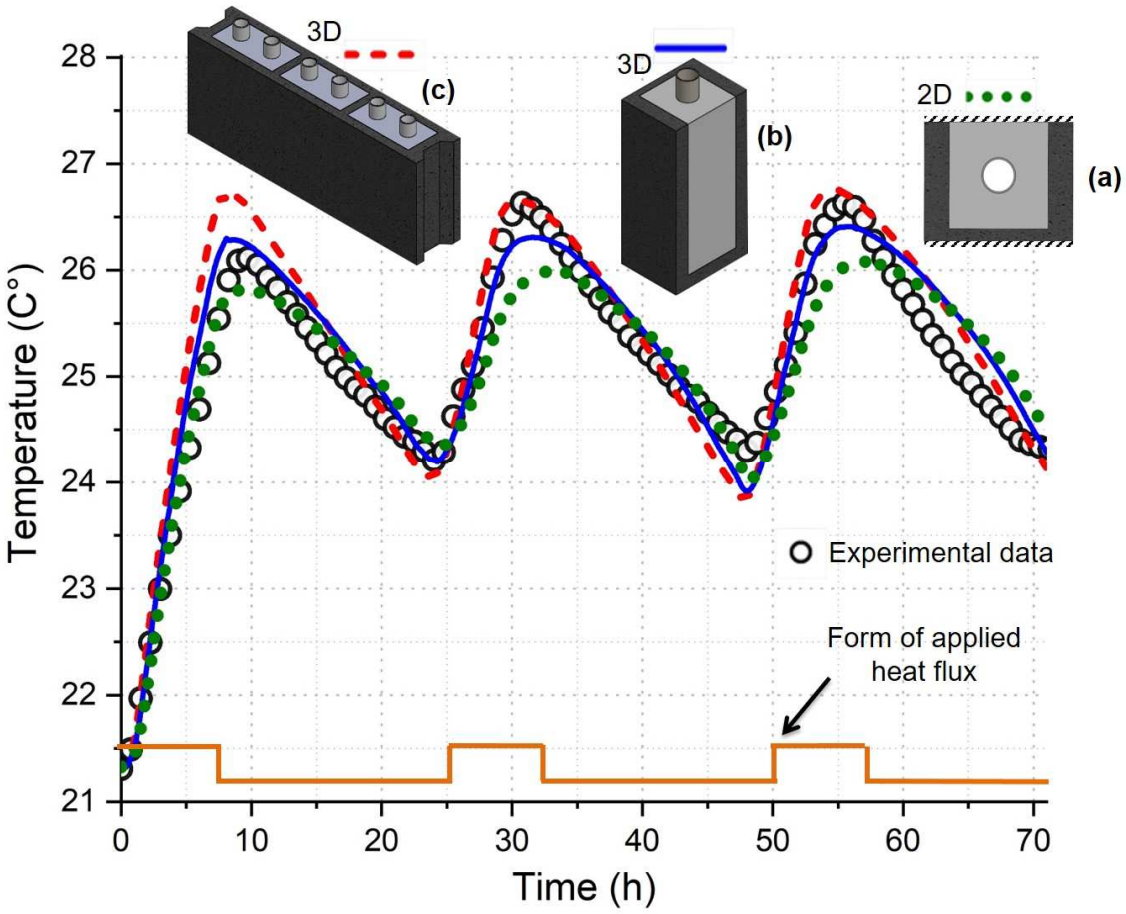

908

909 **Fig. 8.** Evolution of the average temperature on the inner surface for different geometric
910 approaches in the case without ventilation.

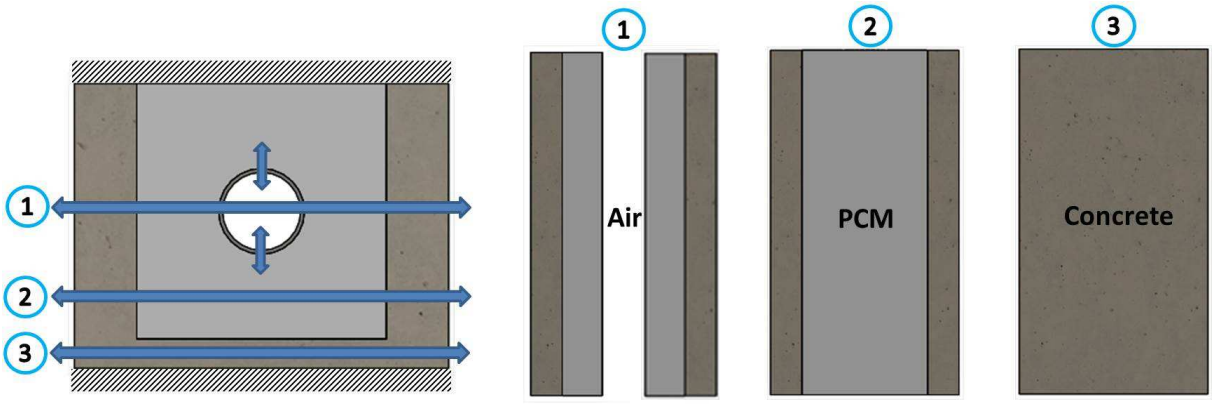

911

912 **Fig. 9.** The configuration of the revealing zone studied according to thermal exchanges.

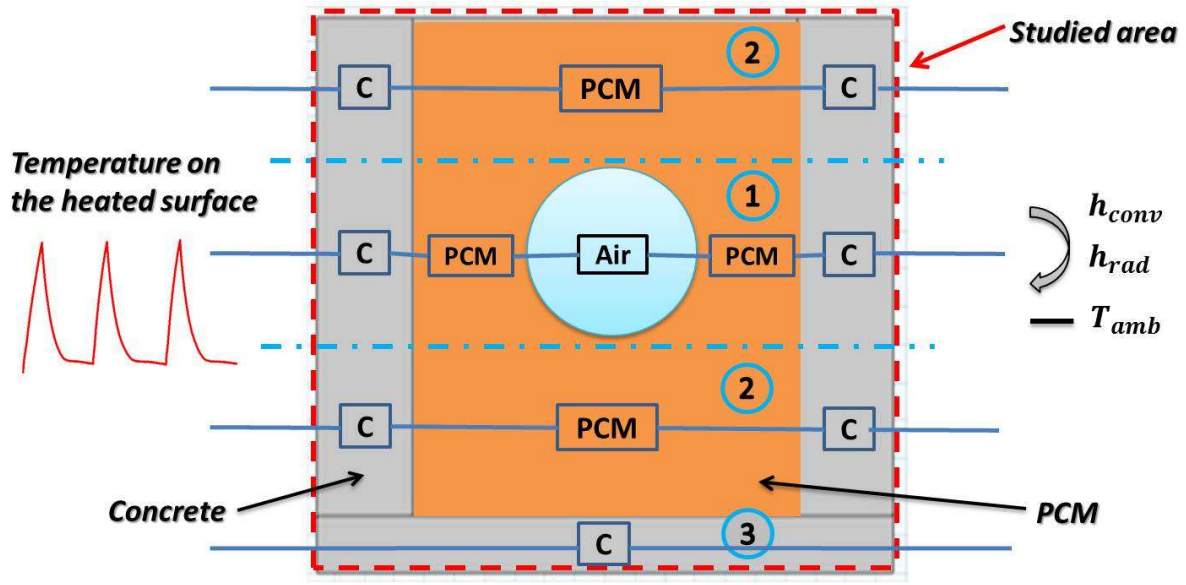

913

914 **Fig. 10.** Equivalent system diagram with the boundary conditions.

915

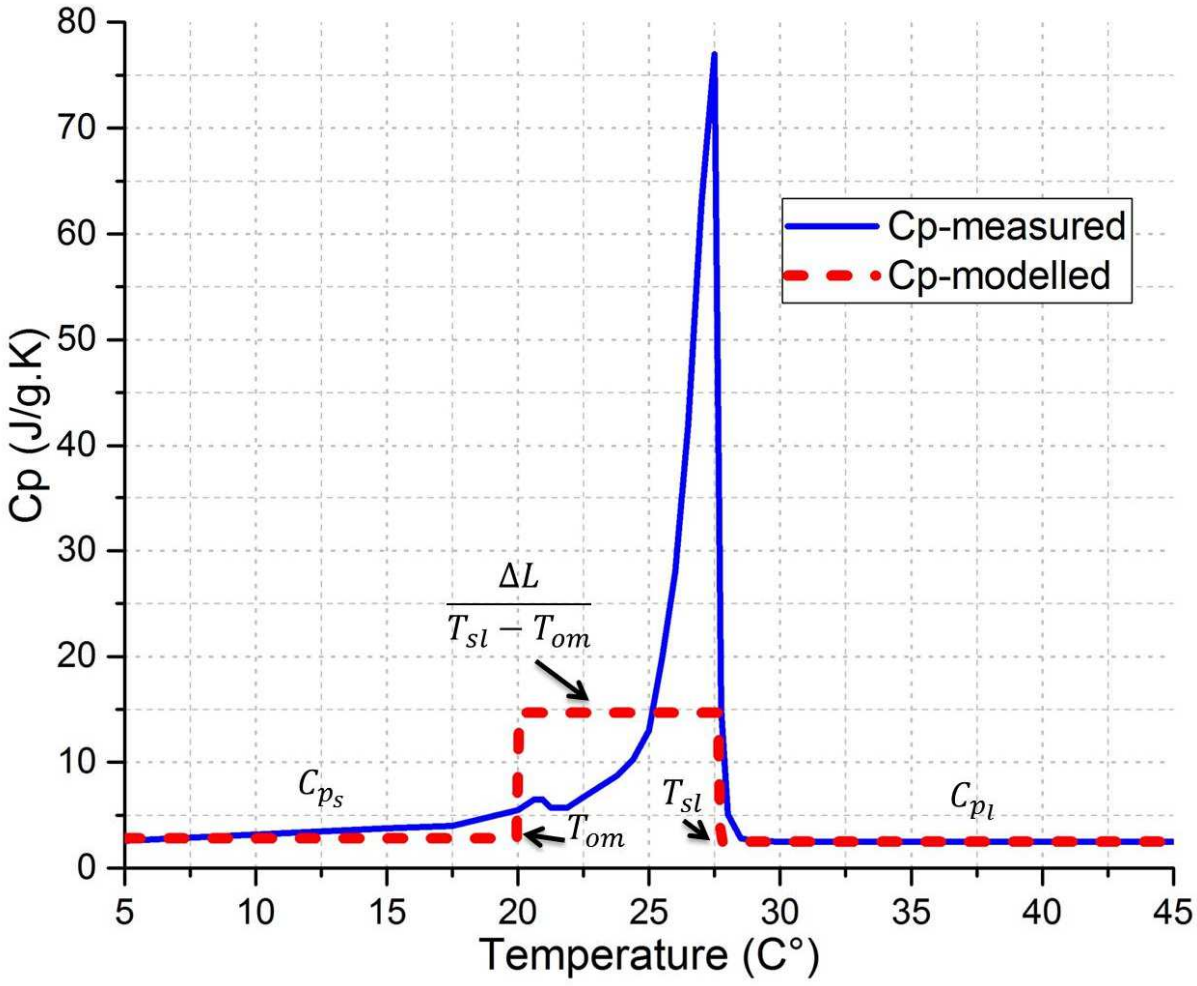

916

917 **Fig.11.** Adopted modelling of the specific capacity of the PCM.

918

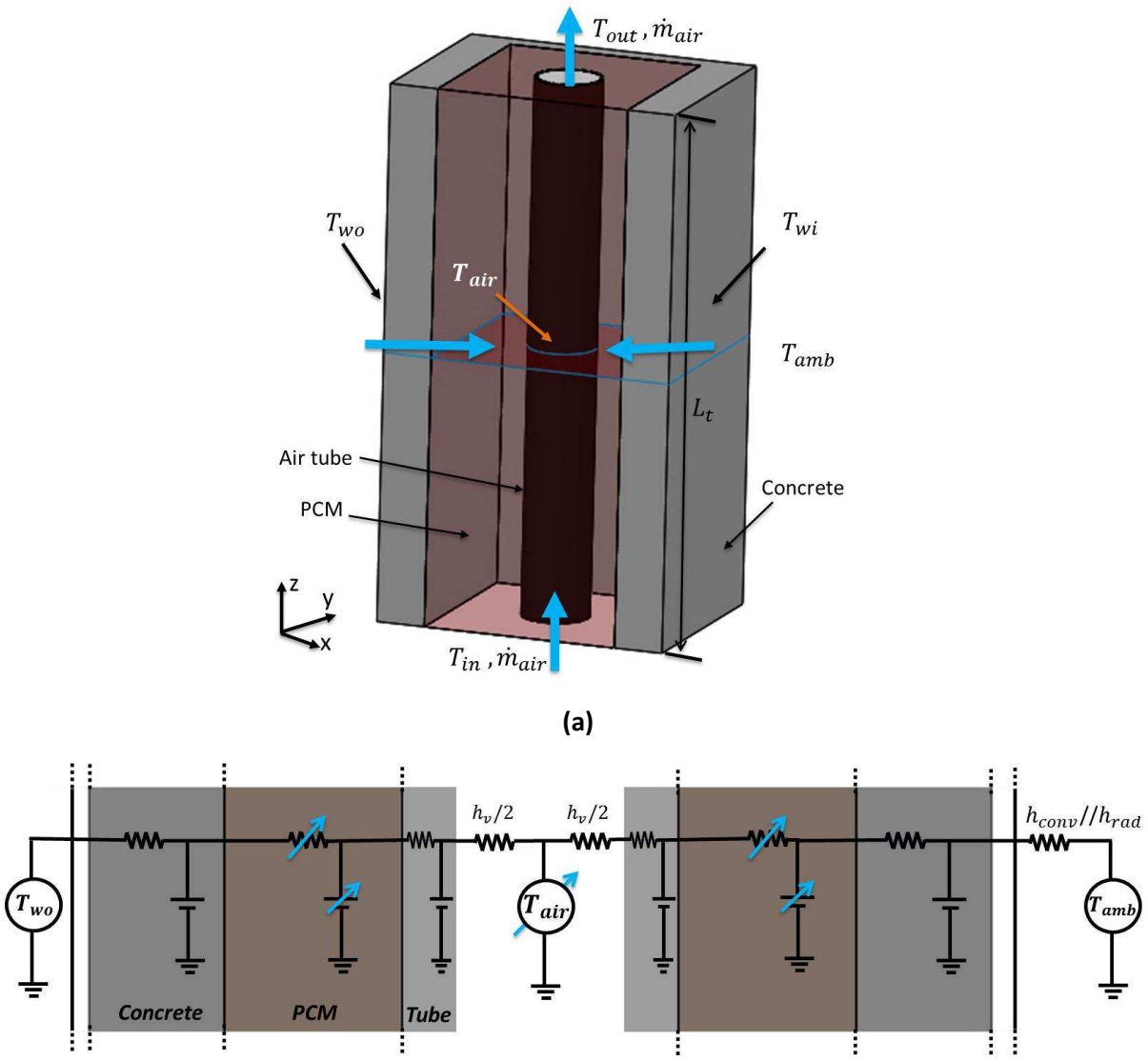

Fig. 12. Airflow modelling through the tube: **(a)** The schematic diagram of modelling parameters, **(b)** Equivalent electrical diagram of the middle part containing the tube.

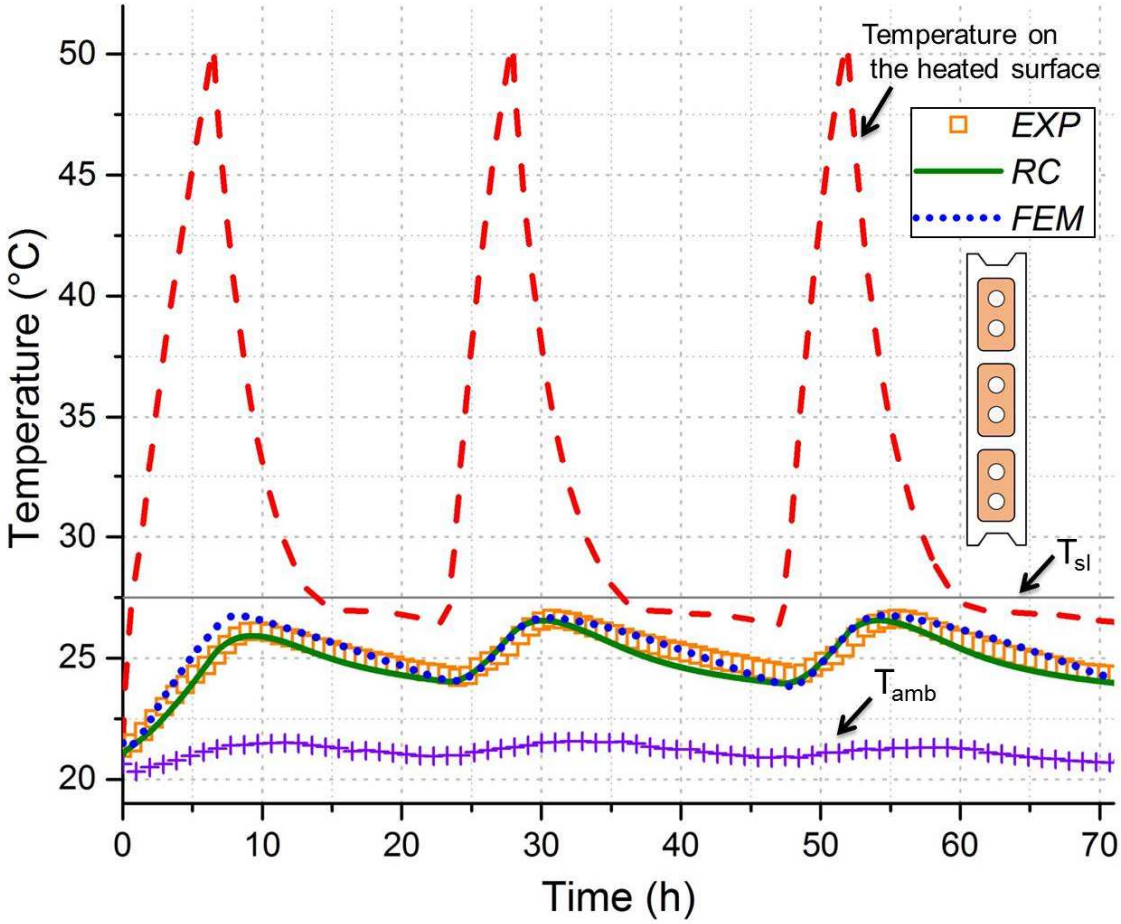
Temperature on
the heated surface
EXP
RC
FEM
T_{sl}
T_{amb}
Temperature (°C)
Time (h)
50
45
40
35
30
25
20
0
10
20
30
40
50
60
70

925

926 **(a)**

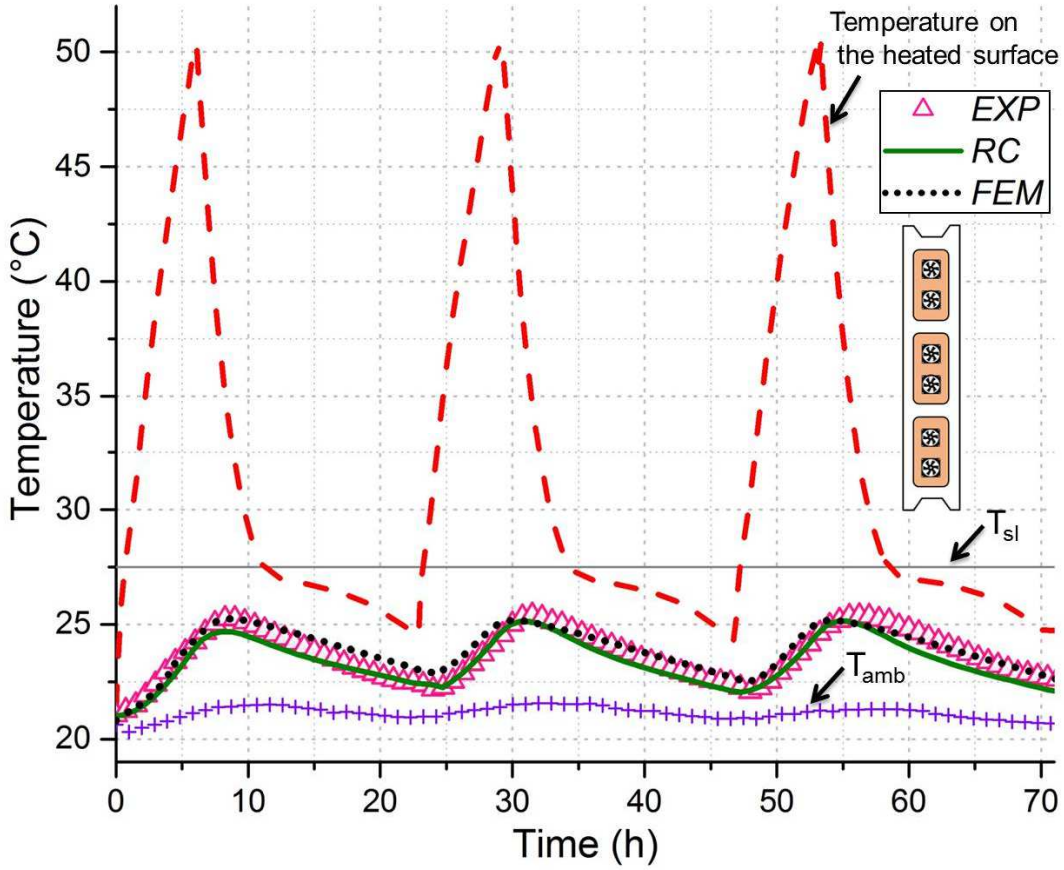

(b)

Fig. 13. Temperature of the surface of the concrete block, comparison of the experimental data with the two models RC and FEM: **(a)** without ventilation, **(b)** with ventilation.